Formation of nanometerscale layers of V-VI (Bi₂Te₃-related) compounds based on amorphous precursors

Harald Böttner[a], Dirk Ebling[a], Heiko Kölbel[a], Axel Schubert[b], Alexander Gavrikov[b], Andreas Mahlke[b] and Joachim Nurnus[b]

[a] Fraunhofer Institut Physikalische Messtechnik, Heidenhofstr. 8, DE-79110 Freiburg, Germany; harald.boettner@ipm.fhg.de
[b] Micropelt GmbH, Emmy-Noether-Str. 2, 79110 Freiburg, Germany

Abstract. Nanometerscale textured layers were achieved by annealing corresponding elemental layers, deposited in nanometerscale thickness which fits to the intended stoichiometry of the resulting compounds. The compound formation as well as the accompanying thermoelectric properties are reported. The compound formation corresponds in particular to the evolution of the Seebeck coefficient.

Key words: thermoelectricity, stoichiometry, textured layer, nanometer scale.

1. INTRODUCTION

It is commonly agreed that superlattices (SLs) of thermoelectrics will allow for outstanding device performance [1]. Due to the required nanometerscale of the individual layers within the SLs, questions about the structural stability may arise. The stability of MOCVD-grown p-type Sb_2Te_3/Bi_2Te_3- and n-type $Bi_2Te_3/Bi_2(Se,Te)_3$-superlattices has already been reported [2]. The stability of SLs, deposited on heated substrates (~200 °C), has also been reported for MBE-grown $Bi_2Te_3/Bi_2(Se,Te)_3$-compound-SLs [3]. A different and new process that was recently reported shows that V-VI materials, deposited at ambient temperature as thin element layers, crystallize almost perfectly oriented during a post-annealing process if suitable diffusion barriers were used between the V_2-VI_3-layers [4]. The practical use of these SL-TE-layers are Peltier coolers for

high (>100 W/cm^2) cooling power densities [5], which can be used as high heat load devices.

High heat load microdevices need a leg height of some 10 μm [6]. Sputtering is one of the best suited deposition techniques for a thickness around 10 μm [2,3].

To suppress interdiffusion during growth, which is Se/Te interdiffusion for *n*-type SLs-Bi$_2$Te$_3$/Bi$_2$(Se,Te)$_3$ alternating layers and Bi/Sb interdiffusion for *p*-type SLs-Sb$_2$Te$_3$/(Bi,Sb)$_2$Te$_3$ as alternating layers, the SLs may be deposited on unheated or even cooled substrates and optimized in a post-annealing process [4]. For the so-called cold sputtered and post-annealed TE-material superior TE-properties have been achieved [5].

For *p*-type sputtered materials better power factors have been reported compared to *n*-type sputtered materials. So it was decided to develop first *n*-type V$_2$-VI$_3$ SLs.

The studies concerning growth, crystallization and evolution of thermoelectric properties of *n*-type V-VI SLs will be reported in this paper. For compound and SL-formation, alternating Bi and Te were deposited to form *n*-Bi$_2$Te$_3$; alternating Bi and (Se,Te) layers were deposited likewise to form Bi$_2$(Se,Te)$_3$. Figure 1 gives a sketch of the deposited layers and the formation of the intended crystalline structures by diffusion processes and expected self-organization of the system.
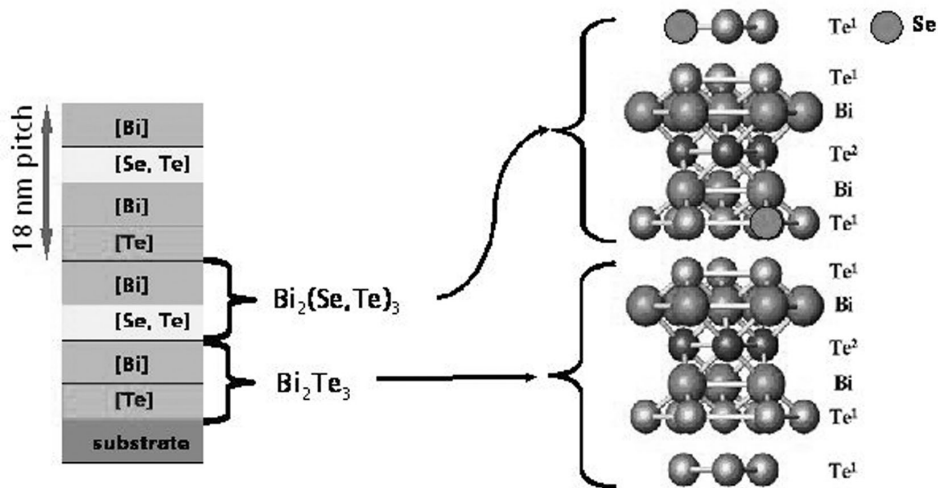

Fig. 1. Deposition and annealing of [Bi/Te/Bi/(Se,Te)]$_n$ stacks for the oriented growth of a Bi$_2$Te$_3$/Bi$_2$(Se,Te)$_3$ SLs, by diffusion and self-organization.

2. EXPERIMENTAL

All layers were fabricated using an Ardenne CS 850 S (Germany) sputter equipment. The layers were deposited from elemental 8″ Bi, Te and Se-targets with 99.995% purity on SiO_2-passivated 4″-Si-wafers and on polished 1 cm^2 BaF_2 pieces. In the case of the intended $Bi_2Te_3/Bi_2(Se,Te)_3$ SLs, the thickness of the individual layers was adjusted down to a range of 4–5 nm by setting the target power and sputter time of the SL-forming layers properly. The layers were structurally characterized using XRD, SIMS and SEM analysis. In addition, thermoelectric properties were measured at room temperature depending on the post-annealing temperatures. The annealing time was 2 h, which was found to be suitable to investigate the main effects for the phase formation and the evolution of the wanted V_2-VI_3 compounds.

3. STRUCTURAL PROPERTIES OF Bi_2Te_3/Bi_2 $(Se,Te)_3$ LAYERS

Layers following the stoichiometry for Bi_2Te_3 and $Bi_2(Se,Te)_3$, were deposited as a stack (Fig. 2), with periods of 100, 45 and 18 nm. By this, the individual layer thickness, measured by BSE analysis, decreases from 25 to about 4–5 nm. Even for the 18 nm period, the individual layers of about 4–5 nm thickness can be identified in Fig. 2 (left) by BSE. According to Fig. 4, the individual layers disappear above a temperature of 150°C due to upcoming interdiffusion processes.

Figure 3 shows the BSE pictures of a 100 nm period as-grown, after annealing at temperatures of 150, 300 and 350°C. For the annealing temperature of 150°C the layered structure of the SLs could still be observed with only small
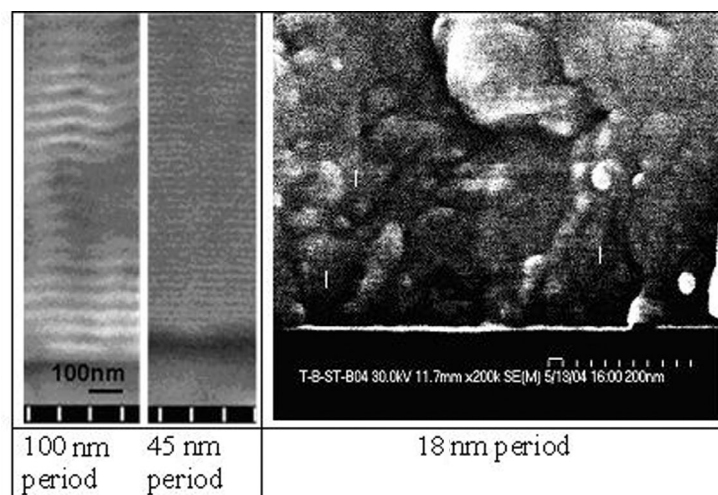

Fig. 2. BSE-pictures of a cleaved cross-section of as-grown $[Bi/Te/Bi/(Se,Te)]_n$ stacks for a $Bi_2Te_3/Bi_2(Se,Te)_3$ SLs, scaling for 100 nm and 45 nm period stack is 100 nm.
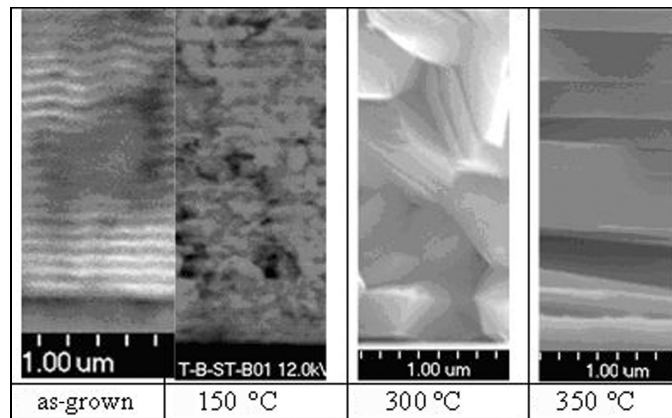
356

Fig. 3. BSE-pictures of a cleaved cross-section of annealed [Bi/Te/Bi/(Se,Te)]$_n$ layers with 100 nm period.

changes due to interface roughening compared to the as-grown stack. As can be seen from Fig. 3, temperatures above 300 °C induce growth of individual grains and the SL-structure vanishes completely. The size and shape are very similar after annealing at 300–350 °C for all three types of stack periods according to Fig. 2 and the results for the 100 nm stack is given as an example in Fig. 3. From the BSE analysis one would expect randomly oriented grains for annealing temperatures above 150 °C.

The as-grown, 150, 300 and 350 °C annealed samples were characterized by XRD. Figure 4 shows the XRD-analysis for a stack with 25 nm thin layers in the conditions as-grown, for 150, 300 and 350 °C annealing temperatures. The evolution of the observed peaks may be explained as follows. Even during deposition, the phase formation takes place at the phase boundaries Bi/(Se,Te) and Bi/Te, indicated by the (006) reflex. That means that thin layers in the nm range of Bi$_2$Te$_3$ and Bi$_2$(Se,Te)$_3$ phases start to form even under the growth conditions, which sandwich the amorphous rest of the Bi, Te and (Se,Te) layers. With rising annealing temperature from 150 to 300 °C, phase formation increases and the crystallization of the remaining elemental layers starts, indicated by the occurrence of a multiplicity of peaks in the XRD diagram. Almost all peaks (compound and elements) could be assigned to the corresponding phases of the materials.

In accordance with Fig. 4, at 350 °C the stacks are oriented in c-direction, which is obviously related to the well defined 00L peaks and by the disappearance of other element and Bi$_2$Te$_3$ like reflexes. The remaining reflexes are shifted compared to pure Bi$_2$Te$_3$ due to the Se-content. Based on Vegard's law [6], the expected average Se-content of 3 at% could be derived from the shift of the reflexes.

The same analysis was performed for the 18 nm period stacks shown in Fig. 5. The high c-orientation shows up already at lower temperatures of about 300 °C,

Fig. 4. XRD-analysis of as-grown and annealed [Bi/Te/Bi/(Se,Te)]$_n$ layers with 100 nm period. In the upper part the hkl-indices for Bi_2Te_3 are given for comparison.

Fig. 5. XRD-analysis of as-grown and annealed [Bi/Te/Bi/(Se,Te)] layers with 18 nm period. In the upper part of Fig. 4 the hkl-indices for Bi_2Te_3 are given for comparison.

accompanied by a smaller amount of "other" reflexes and even more intensive 00L reflexes at lower temperatures. The growth of the final V-VI layer is limited to about 1/6 of the thickness compared to the 100 nm period stack until the elemental source layers are "consumed" for the layer growth of the compound material.

The observation that the V-VI layers start to grow at lower temperatures or even during growth on non-heated substrates by reducing the period length of the stacks, indicates that the diffusion of the specimen through the already formed layers is not the (only) rate determining step of the solid state reaction. Rather it is to be taken into account that nucleation processes or other transport phenomena influence the reaction rate considerably, which is also expressed by the high amount of orientation along the c-axis. Further studies of the solid state reaction mechanisms are necessary to elucidate these processes in greater detail.

4. ELECTRICAL AND THERMOELECTRICAL PROPERTIES

The electrical properties like the electrical conductivity σ [Ω^{-1} cm^{-1}], the carrier concentration n [cm^{-3}] and the carrier mobility μ [Vsec/cm^2] as well as the thermoelectrical "performance" by the Seebeck coefficient S [μV/K], were measured at the room temperature. The power factor $PF = S^2\sigma$, instead of the commonly used figure of merit Z, has been taken to characterize the quality of the material.

The increase of the Seebeck coefficient with rising annealing temperature (Fig. 6) is in accordance with the concluded phase formation at about 100–150°C. No significant difference can be observed between different layer types. At an
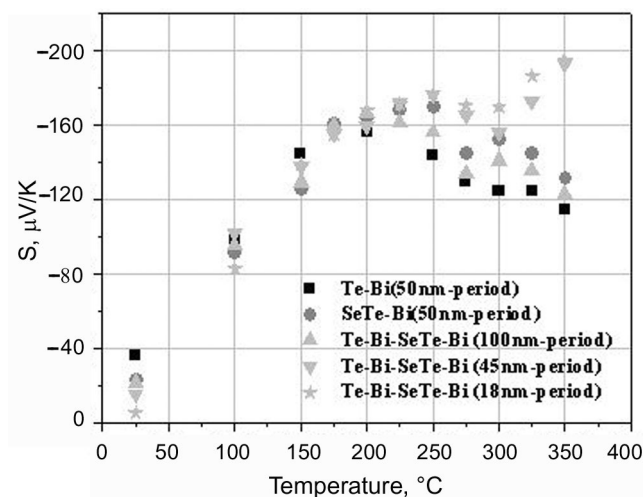

Fig. 6. Dependence of the Seebeck coefficient S on annealing temperature for different layers.

annealing temperature of about 220 °C all layers reach an intermediate maximum for the Seebeck coefficient at almost the same point. It is remarkable that above 220 °C, Bi_2Te_3, $Bi_2(Se,Te_3)$ and the $Bi_2Te_3/Bi_2(Se,Te)_3$ stack with 100 nm periods show similar behaviour, whereas the $Bi_2Te_3/Bi_2(Se,Te)_3$ SLs with the 45 and 18 nm periods differ significantly from the others. The Seebeck coefficient is again increasing. The development of the Seebeck coefficient with the temperature may be interpreted as follows. The phase formation starts at around 150 °C. The start of the phase formation is accompanied by the evolution of the Seebeck coefficient, what is typical for this *n*-type material. This assumption is supported by the fact that the carrier concentration decreases continuously with the tendency to stabilize at about 200 °C. In addition, the carrier mobility raises steadily (not shown here).

The decrease of the Seebeck coefficient above 220–250 °C for Bi_2Te_3, $Bi_2(Se,Te)_3$ and the $Bi_2Te_3/Bi_2(Se,Te)_3$ stack with 100 nm periods may be caused by to the grain growth, which induces a decrease to the grain boundary scattering. The increase of the Seebeck coefficient in spite of the grain growth for the 45 and 18 nm period material may be caused by the low temperature c-orientation (Fig. 5). Again one possible reason might be the short distance for a complete and perfect interdiffusion, in particular for the stack with 4–5 nm thin layers. The resulting power factor is plotted in Fig. 7. Reasonable power factors for short $[Bi_2Te_3/Bi_2(Se,Te)_3]_n$-periods (45 and 18 nm) in particular were derived.
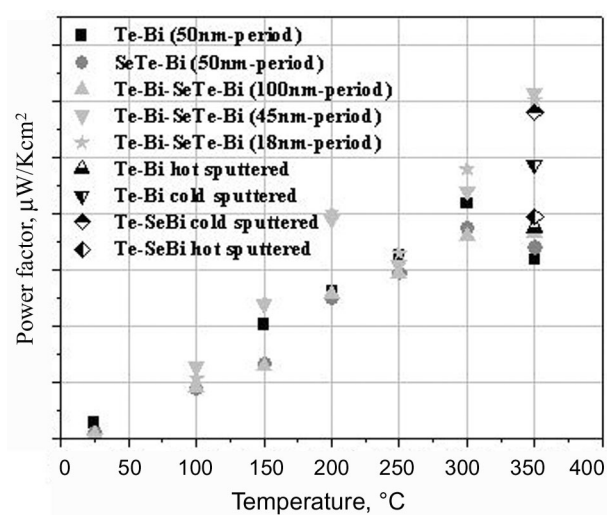

Fig. 7. Dependence of the power factor on annealing temperature of different layers.

5. CONCLUSIONS

For the development of sputtered SLs, three types of layered stacks were deposited: [Bi/Te]$_n$, [Bi/(Se,Te)]$_n$ as constituents and the resulting SL [Bi/Te/Bi/(Se,Te)]$_n$. An individual layer thickness down to 4–5 nm was realized, which should significantly reduce the thermal conductivity for the resulting 9 nm SL-layers. The successful deposition of nm-thin layers was proven by BSE-analysis. Phase formation starts even at deposition close to the interface and/or for thinner stacks. The evolution of thermoelectric properties, which depend on the annealing temperature, in particular the Seebeck coefficient, is in close accordance to the phase formation of the V$_2$-VI$_3$ staggered layers as shown by XRD analysis. The mechanism and the rate determining step of the solid state reaction of the the growth process is still unsolved and needs further investigation. The annealing of the layers improves the Seebeck coefficient for all kind of layers considerably.

REFERENCES

1. Harman, T. C., Taylor, P. J., Walsh, M. P. and La Forge, B. E. Quantum Dot superlattice materials and devices. *Science*, 2002, **297**, 2229–2232.
2. Venkatasubramanian, R., Siivola, E., Colpitts, T. and O'Quinn, B. Thin-film thermoelectric devices with high room-temperature figures of merit. *Nature*, 2001, **413**, 597–602.
3. Lambrecht, A., Beyer, H., Nurnus, J., Künzel, C. and Böttner, H. High figure of merit ZT in PbTe and Bi$_2$Te$_3$ based superlattice structures by thermal conductivity reduction. In *Proc. 20th International Conference on Thermoelectrics*. Beijing, 2001, 335–339.
4. Harris, F. R., Standridge, S., Feik, C. and Johnson, D. C. Design and synthesis of [(Bi$_2$Te$_3$)x(TiTe$_2$)y] super-lattices. *Angew. Chem. Int. Engl.*, 2003, **42**, 5295–5299.
5. Böttner, H., Nurnus, J., Gavrikov, A., Kühner, G., Jägle, M., Künzel, C., Eberhard, D., Plescher, G., Schubert, A. and Schlereth, K.-H. New thermoelectric components using microsystem technologies. *IEEE J. Microelectromech. Syst.*, 2004, **13**, 414–420.
6. Nurnus, J., Künzel, C., Beyer, H. et al. Structural and thermoelectric properties of Bi$_2$Te$_3$ based layered structures. In *Proc. 19th International Conference on Thermoelectrics*. Cardiff, 2000, 236–240.
7. Fleurial, J.-P., Borshchevsky, A., Ryan, M. A., Phillips, W., Kolawa, E., Kacisch, T. and Ewell, R. Thermoelectric microcoolers for thermal management applications. In Proc. 16th International Conference on Thermoelectrics. Dresden, 1997, 641–645.

Amorfsete prekursorite baasil moodustatud V-VI (Bi$_3$Te$_3$) ühendite nanomeeterskaalasse kuuluvate kihtide formeerumine

Harald Böttner, Dirk Ebling, Heiko Kölbel, Axel Schubert, Alexander Gavrikov, Andreas Mahlke ja Joachim Nurnus

Nanomeeterskaalas moodustatakse tekstuuriga kihid algsete kihtide noolutuse abil, mis viib need vastavusse saadavate ühendite kavandatud stoikomeetriaga. On käsitletud ühendite moodustumist koos nende termoelektriliste omaduste muutumisega, kusjuures erilist tähelepanu on pööratud ühendite moodustumisega kaasnevale Seebecki teguri evolutsioonile.